

Wavelength- and structure-insensitive on-chip mode manipulation based on the Thouless pumping mechanism

Yingdi Pan,^a Lu Sun^{✉,a,*}, Jingchi Li,^a Qiyao Sun,^a Pan Hu,^a Songyue Liu,^a Qi Lu,^a Xiong Ni,^a Xintao He,^b Jianwen Dong,^{b,*} and Yikai Su^{a,*}

^aShanghai Jiao Tong University, State Key Lab of Advanced Optical Communication Systems and Networks, Department of Electronic Engineering, Shanghai, China

^bSun Yat-sen University, School of Physics, State Key Laboratory of Optoelectronic Materials and Technologies, Guangzhou, China

Abstract. Coupled-waveguide devices are essential in photonic integrated circuits for coupling, polarization handling, and mode manipulation. However, the performance of these devices usually suffers from high wavelength and structure sensitivity, which makes it challenging to realize broadband and reliable on-chip optical functions. Recently, topological pumping of edge states has emerged as a promising solution for implementing robust optical couplings. In this paper, we propose and experimentally demonstrate broadband on-chip mode manipulation with very large fabrication tolerance based on the Rice–Mele modeled silicon waveguide arrays. The Thouless pumping mechanism is employed in the design to implement broadband and robust mode conversion and multiplexing. The experimental results prove that various mode-order conversions with low insertion losses and intermodal crosstalk can be achieved over a broad bandwidth of 80 nm ranging from 1500 to 1580 nm. Thanks to such a topological design, the device has a remarkable fabrication tolerance of ± 70 nm for the structural deviations in waveguide width and gap distance, which is, to the best of our knowledge, the highest among the coupled-waveguide mode-handling devices reported so far. As a proof-of-concept experiment, we cascade the topological mode-order converters to form a four-channel mode-division multiplexer and demonstrate the transmission of a 200-Gb/s 16-quadrature amplitude modulation signal for each mode channel, with the bit error rates below the 7% forward error correction threshold of 3.8×10^{-3} . We reveal the possibility of developing new classes of broadband and fabrication-tolerant coupled-waveguide devices with topological photonic approaches, which may find applications in many fields, including optical interconnects, quantum communications, and optical computing.

Keywords: topological photonics; Thouless pumping; coupled-waveguide device; on-chip mode manipulation.

Received Mar. 2, 2025; accepted for publication Apr. 15, 2025; published online May 11, 2025.

© The Authors. Published by SPIE and CLP under a Creative Commons Attribution 4.0 International License. Distribution or reproduction of this work in whole or in part requires full attribution of the original publication, including its DOI.

[DOI: [10.1117/1.APN.4.3.036012](https://doi.org/10.1117/1.APN.4.3.036012)]

1 Introduction

Coupled-waveguide devices play a pivotal role in photonic integration for their wide applications in power coupling,^{1,2} polarization beam splitting and rotation,³ and mode conversion and multiplexing.^{4,5} However, the coupling between different waveguides and modes usually suffers from high wavelength

and structure sensitivity. Stringent nanofabrication precision is required for achieving qualified devices, which limits the yield and the scale of the integrated photonic circuits. Therefore, broadband and structure-insensitive coupled-waveguide devices based on naturally robust physical mechanisms are very much desired in large-scale photonic integration and massive production.

With its emergence, topological photonics has attracted great interest for the robust transport of light enabled by the topological edge states (TESSs). TESSs, which are protected by the

*Address all correspondence to Lu Sun, sunlu@sjtu.edu.cn; Jianwen Dong, dongjwen@mail.sysu.edu.cn; Yikai Su, yikaisu@sjtu.edu.cn

topologically nontrivial phases, have demonstrated their robustness against disorders and imperfections⁶ in a variety of circumstances, such as polarization conversion,⁷ nonlinear light generation,⁸ and topological insulator lasers.⁹ Robust waveguiding, coupling, and splitting of TESs in coupled-waveguide structures have also been experimentally demonstrated in Su–Schrieffer–Heeger (SSH) modeled silicon waveguide arrays¹⁰ and Floquet gauge engineered silicon waveguide arrays.¹¹ These structures are insensitive to the variations in wavelength and gap distance among silicon waveguides to some degree. However, they are still vulnerable to the structural variation in waveguide width.^{10–12}

Thouless pumping is another example of topology. When the parameters in a Thouless pumping system undergo a cyclic adiabatic evolution, the net particle transfer per cycle is determined by the Chern number of the energy band occupied by the particle.^{13,14} By employing such a topological pumping mechanism, robust excitation transfer has been realized in various physical systems, including ultracold atoms in optical lattices,^{15,16} optical waveguide arrays,^{17–19} and artificial spin systems.^{20,21} Recently, we have proposed and experimentally demonstrated broadband and robust power coupling and mode-order conversion based on the Thouless pumping mechanism in Rice–Mele (RM)-modeled silicon waveguide arrays, which shows significant advantages in expanding the working bandwidth and enhancing the fabrication tolerance of the device.²² However, only a proof-of-concept experiment was carried out for the two lowest-order modes. The method has not been applied to the mode conversion or multiplexing involving more and higher-order modes, which are the key to realizing robust and more complicated on-chip mode manipulation.

Here, we prove the universality of the design method based on the Thouless pumping mechanism by extending the investigation to higher-order modes and accomplishing broadband and fabrication-tolerant mode couplings among arbitrary modes. As compared with other topological waveguide arrays reported previously,^{10,11} the adiabatic pumping scheme used here is more advantageous because it shows robustness against the structural deviations in both waveguide width and gap distance. To characterize the insertion loss (IL) and intermodal crosstalk (CT) of the topological design, we cascade various mode-order converters based on the Thouless pumping mechanism to form a four-channel mode-division multiplexer. The experimental results prove that the proposed multiplexer exhibits low ILs of <2.6 dB and CT values of <−20.5 dB over an 80-nm bandwidth (1500 to 1580 nm) for all four mode channels. Structural parameter discrepancies were also intentionally introduced to the topological structure and its conventional counterpart based on asymmetric directional couplers (ADCs) to compare the fabrication tolerance of these two kinds of designs. The topological device shows a great fabrication tolerance of ±70 nm for the structural deviations in waveguide width and gap distance, whereas the performance of the conventional device deteriorates rapidly with the structural parameters deviating from the designed values. To the best of our knowledge, the proposed device has the highest fabrication tolerance among the coupled-waveguide mode-handling devices that have ever been reported in literature. Moreover, we carry out a mode-division multiplexing (MDM) experiment to demonstrate the performance of the proposed devices in high-speed data transmission of 16-quadrate amplitude modulation (16-QAM) signals. The transmission capacity per lane reaches 200 Gbit/s, with the bit error

rates (BERs) below the 7% forward error correction (FEC) threshold of 3.8×10^{-3} . To the best of our knowledge, this is the first demonstration of the robust transmission of data in a high-speed topological MDM system. Our approach provides a one-time solution for broadening the working bandwidth and loosening the fabrication accuracy requirement for on-chip mode manipulation, which may open a new avenue toward the practical applications of topological photonics in diverse fields such as optical communications,^{23,24} quantum information processing,^{25,26} and large-scale neural networks.^{27,28}

2 Principles and Methods

2.1 Topological Pumping of Edge States in the RM Model

The RM model is realized by an array of evanescently coupled silicon waveguides fabricated on the silicon-on-insulator (SOI) platform (3- μm -thick buried oxide layer, 220-nm-thick silicon top layer, and 1- μm -thick silica upper cladding layer), as schematically illustrated in Fig. 1(a). The waveguide array resembles a Su–Schrieffer–Heeger (SSH) lattice in the transverse direction with the narrow and wide waveguides in the bipartite unit cell of the waveguide array supporting the fundamental and high-order modes, respectively. The neighboring lattice sites share the same on-site energy, i.e., the fundamental mode in the narrow waveguide and the high-order mode in the wide waveguide must have equal effective modal indices. The waveguide widths and the gap distances among the waveguides change periodically along the propagation direction in such a way that the dynamics of light propagation in the system can be described by the tight-binding Hamiltonian of the RM model.^{13,29–31}

$$H = \frac{1}{2} h(z) \sum_i (-1)^i c_i^\dagger c_i + \frac{1}{2} \sum_i [\tau + (-1)^i \delta(z)] c_i^\dagger c_{i+1} + h.c., \quad (1)$$

where c_i^\dagger and c_i are the creator and annihilator on lattice site i , τ is the uniform coupling strength, and z is the propagation distance normalized to the periodicity L along the propagation direction. $h(z) = h_0 \sin 2\pi z$ and $\delta(z) = e^{\delta_0 \cos 2\pi z} - 1$ are the periodic modulations of the mode mismatching and coupling strengths, respectively, which can be obtained by varying the waveguide widths and the gap distances (see Sec. S2 in the [Supplementary Material](#) for details). As an example, here we consider the transverse magnetic (TM) modes in an array consisting of 30 waveguides with alternating widths. The narrow waveguides support the TM_0 mode, the effective index of which matches that of the TM_1 mode in the wide waveguides. The band structure of the TM supermodes in such an array over a full pump cycle is shown in Fig. 1(b). A pair of edge states appears in the bandgap, which is represented by the red and blue solid lines in the band diagram. Different from the normal RM model, where the periodic on- and off-site modulations $h(z)$ and $\delta(z)$ are typically sinusoids, the evanescent couplings among neighboring waveguides in our design lead to a “lopsided” RM Hamiltonian, and therefore the asymmetric band structure is shown in Fig. 1(b). In Fig. 1(c), we display the mode profiles of the supermodes at Points IA to VIIIA (Points IB to VIIIB) along the blue (red) curve in Fig. 1(b). Panels IA to VIIIA correspond to the mode evolution on the blue curve. The mode is initially located in the bandgap and is highly localized on the left

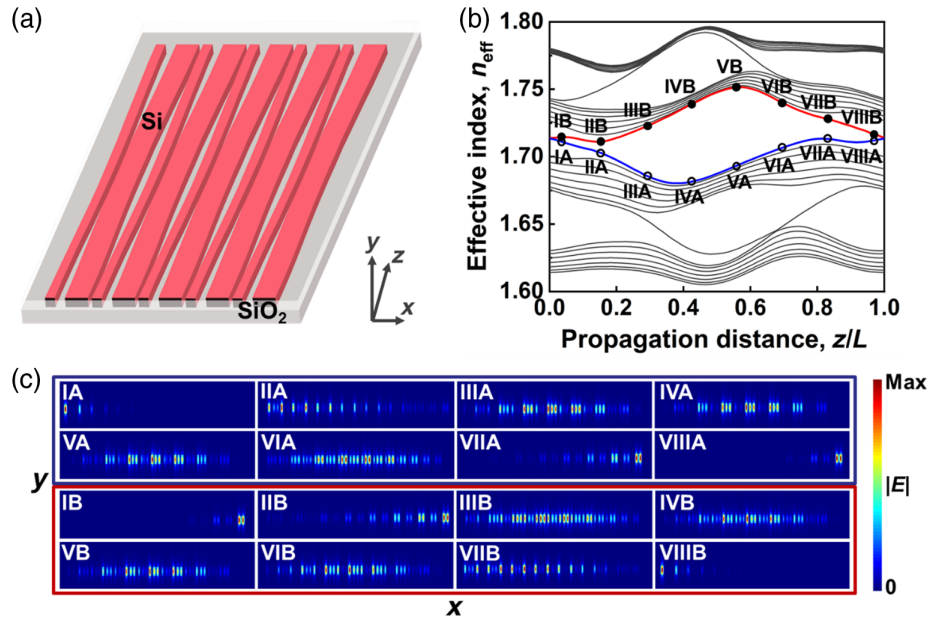


Fig. 1 Thouless pumping process in an RM-modeled silicon waveguide array. (a) Schematic of the coupled-waveguide array. (b) Band structure of the TM supermodes in an array of 30 waveguides with alternating widths. The black solid lines represent the bulk bands, whereas the red and blue solid lines represent the left and right edge states when $z \in [0, 1/4) \cup (3/4, 1]$. (c) Mode profiles ($|E|$) of the supermodes at Points IA to VIII A (Points IB to VIII B) on the blue (red) curve in panel (b).

edge of the waveguide array. Then, it approaches the bulk bands and becomes extended in the middle waveguides. Finally, it returns to the bandgap and gets localized on the right edge, completing the edge-to-edge transport of light and the conversion from the TM_0 mode to the TM_1 mode in one pump cycle. Panels IB to VIII B illustrate the mode evolution along the red curve in Fig. 1(b), where the TM_1 mode launched from the right edge transports to the left edge and becomes the TM_0 mode in the adiabatic pumping process. Most importantly, the edge-to-edge transport of light and the mode conversion are topologically protected by the Chern number. When the closed loop of the modulations in the (h, δ) -space encircles the origin, the Chern number is equal to 1 and the edge state traverses the bulk and populates the edge state on the other side of the lattice. When the region encircled by the loop does not contain the origin, the Chern number equals 0, and the Thouless pumping process does not occur. By exploiting the topological nature of this process, one can implement robust on-chip mode manipulation that is insensitive to the variations in wavelength and structural parameters to a large extent. More details about the analytical expression of the edge states in the waveguide array and the explanation of the robustness originating from the Thouless pumping mechanism can be found in Sec. S1 in the [Supplementary Material](#).

2.2 Mode Conversions Based on the Thouless Pumping Mechanism

We start with different kinds of mode-order conversions in the topological waveguide arrays to prove the feasibility of on-chip mode manipulation using the Thouless pumping mechanism. To achieve a compact device footprint, we adopt the simplest structures with only four waveguides to realize the Thouless

pumping process and the mode-order conversion. The topological protection of the edge-to-edge transport still exists with only a few waveguides as long as the parametric loop in the (h, δ) -space encircles the origin point. A more detailed explanation can be found in Sec. S1 in the [Supplementary Material](#). The mode conversion region is illustrated in Fig. 2(a) with the bottom narrow and top wide waveguides supporting the fundamental mode (TM_0) and high-order modes ($TM_{1,2,3}$), respectively. To exploit the topological pumping mechanism, the waveguide widths and the gap distances among neighboring waveguides in the mode conversion region change gradually along the propagation direction to realize the mode mismatching strength $h(z)$ and the mode coupling strength $\delta(z)$ in Eq. (1) (see Sec. S2 in the [Supplementary Material](#)). To reach the phase matching condition between the fundamental mode and different high-order modes, the widths of the narrow and wide waveguides are designed to vary around the average values of \bar{w}_1 and \bar{w}_2 , respectively, for different mode-order conversions, as listed in Table 1. The mode mismatching strengths are controlled by the waveguide width variations Δw_1 and Δw_2 (the variation ranges are shown in Table 1) so that the effective indices of the TM_0 to TM_3 modes are modulated in the same range of 1.69 to 1.72. The gaps among neighboring waveguides are slowly varied around the average values of \bar{g} by an amount of Δg to accomplish the coupling strength modulations, as shown in Table 1. Based on the even- and odd-mode analysis, we find that the mode coupling strengths change in the range of $0.017k_0$ to $0.075k_0$, $0.011k_0$ to $0.052k_0$, and $0.008k_0$ to $0.041k_0$ for the TM_0 -to- TM_1 , TM_0 -to- TM_2 , and TM_0 -to- TM_3 couplings, respectively, where k_0 is the wave number of light in vacuum at 1550 nm (see Sec. S2 in the [Supplementary Material](#)). The lengths of the mode conversion regions or equivalently the periodicities of the pump cycle L are chosen to be much longer

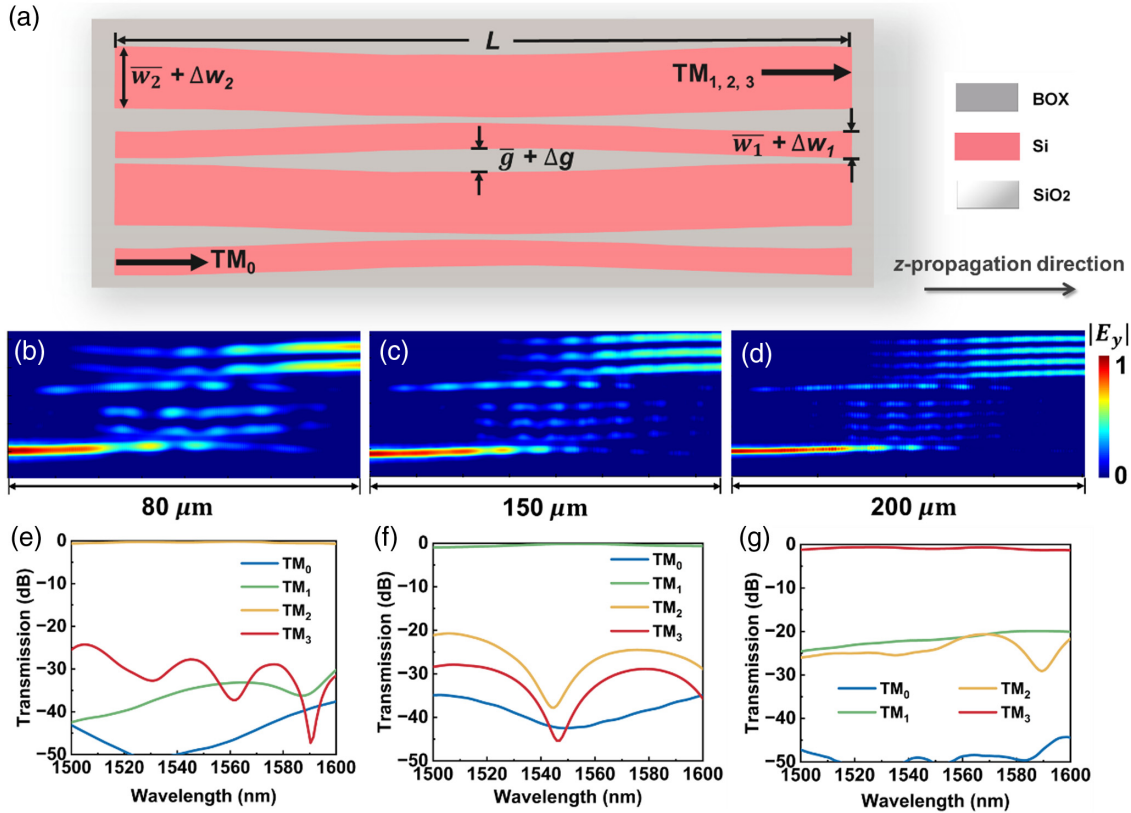


Fig. 2 Mode conversions based on the topological waveguide array. (a) Schematic of the mode conversion region composed of the topological waveguide array. (b)–(d) Light propagation profiles ($|E_y|$) at 1550 nm for the (b) TM_0 -to- TM_1 , (c) TM_0 -to- TM_2 , and (d) TM_0 -to- TM_3 mode conversions when the TM_0 mode is launched from the bottom narrow waveguide. (e)–(g) Simulated transmission spectra of different modes at the output ends of the (e) TM_0 -to- TM_1 , (f) TM_0 -to- TM_2 , and (g) TM_0 -to- TM_3 coupling regions in panels (b)–(d).

than the coupling lengths for the average coupling strength τ in order for the evolution of the TM modes to reach the adiabatic regime, as one can see in Table 1. Note that the minimum feature size of the design (the waveguide width and gap distance) is larger than 130 nm, which means it could be fabricated with foundry-compatible processes.

The full-wave numerical simulations of the mode-order conversions in the topological waveguide arrays were performed using the three-dimensional finite-difference time-domain (3D FDTD) methods. Figures 2(b)–2(d) display the light propagation profiles ($|E_y|$) at 1550 nm for the TM_0 -to- TM_1 , TM_0 -to- TM_2 , and TM_0 -to- TM_3 coupling regions, respectively. The TM_0 mode is launched from the bottom narrow waveguide, experiences the topological pumping process shown in Figs. 1(b) and 1(c), and finally outputs from the top wide waveguide as a high-order mode. The mode overlapping constants between the

output fields and the eigenmode fields are calculated to evaluate the IL and CT levels (see Sec. S2 in the [Supplementary Material](#)). Figures 2(e)–2(g) present the simulated transmission spectra of different modes for the mode conversion regions shown in Figs. 2(b)–2(d). The ILs are lower than 0.67, 0.97, and 1.33 dB, and the CT values are below -20.7 , -24.2 , and -20.0 dB over a 100-nm bandwidth (1500 to 1600 nm) for the TM_0 -to- TM_1 , TM_0 -to- TM_2 , and TM_0 -to- TM_3 conversions, respectively.

To prove the robustness of the mode-order conversions enabled by the Thouless pumping process, we compare the designs based on the topological waveguide arrays with those based on the conventional ADCs. The ADCs consist of a single-mode waveguide (420-nm-wide) and a multimode waveguide (1110-, 1770-, and 2450-nm-wide for the TM_1 , TM_2 , and TM_3 modes, respectively). The coupling lengths are chosen

Table 1 Design parameters for different mode-order conversions.

Mode-order conversion	\bar{w}_1 (nm)	Δw_1 (nm)	\bar{w}_2 (nm)	Δw_2 (nm)	\bar{g} (nm)	Δg (nm)	L (μm)
TM_0 -to- TM_1	420	[−30, 30]	1110	[−45, 45]	300	[−170, 170]	80
TM_0 -to- TM_2	420	[−45, 45]	1770	[−81, 81]	340	[−180, 180]	150
TM_0 -to- TM_3	420	[−35, 35]	2450	[−63, 63]	385	[−200, 200]	200

to be equal to those of the topological designs, i.e., L in Table 1, for a fair comparison. The gaps between the single-mode and multimode waveguides are 840, 500, and 685 nm, respectively, for the TM_0 -to- $TM_{1,2,3}$ ADCs (see Sec. S3 in the [Supplementary Material](#) for more details). We introduce the gap distance deviation (δg for all the gaps) and the waveguide width deviation (δw for the narrow waveguides and $1.7\delta w$, $2.3\delta w$, and $3.1\delta w$ for the wide waveguides supporting the TM_1 to TM_3 modes, respectively) to the topological and conventional structures to investigate the fabrication tolerance of both designs. The width deviations of the wide waveguides are larger than those of the narrow waveguides to meet the phase matching conditions between the fundamental mode and the high-order modes. Figures 3(a)–3(f) show the simulated transmission of the target modes (TM_1 to TM_3) at 1550 nm as functions of waveguide width deviation δw [Figs. 3(a)–3(c)] and gap distance deviation δg [Figs. 3(d)–3(f)]. The ILs of the topological devices are maintained below 2 dB even for very large errors (-75 to 85 nm for δw and -100 to 150 nm for δg), whereas the conventional ones drop very quickly with increasing deviations. The comparison shows clear evidence that the mode-order conversions based on the Thouless pumping process are much more tolerant to the structural discrepancies in both waveguide width and gap distance. Figures 3(g)–3(i) compare the simulated transmission

spectra of the target modes of both the topological and conventional mode-order converters. The 2-dB bandwidths of the conventional devices are narrower than 33 nm which are more than 3 times smaller than their topological counterparts. Therefore, we can conclude that the topological designs have better robustness against wavelength variation compared with the conventional ones, which is very beneficial for achieving ultra-broadband integrated photonic devices.

3 Results and Discussion

3.1 Device Fabrication and Characterization

To characterize the ILs and intermodal CT, the proposed mode-order converters based on the Thouless pumping mechanism and their conventional counterparts based on the ADCs were then cascaded to form the four-channel mode-division multiplexers, as shown in Fig. 4(a). The devices were fabricated on an SOI wafer (3- μm -thick buried oxide layer, 220-nm-thick silicon top layer, and 1- μm -thick silica upper cladding layer) with complementary metal-oxide semiconductor-compatible fabrication processes. The device structures were patterned using E-beam lithography and etched by inductively coupled plasma dry etching. The silica upper cladding layer was

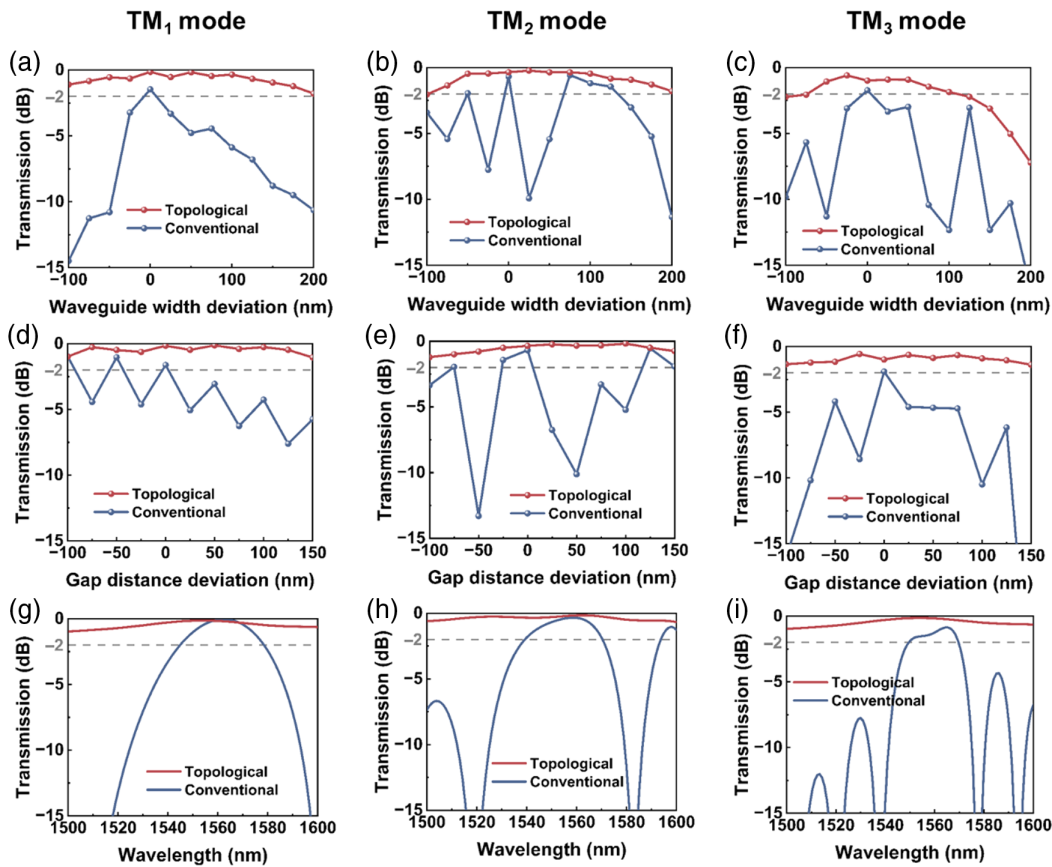


Fig. 3 Comparison of the topological and conventional mode-order conversions. (a)–(f) Simulated transmission of the target modes (TM_1 – TM_3) at 1550 nm when (a)–(c) the waveguide width deviation δw varies from -100 to 200 nm, or (d)–(f) the gap distance deviation δg varies from -100 to 150 nm. (g)–(i) Simulated transmission spectra of the target modes in different mode-order converters. The left, middle, and right columns of the figure correspond to the TM_0 -to- TM_1 , TM_0 -to- TM_2 , and TM_0 -to- TM_3 conversions, respectively.

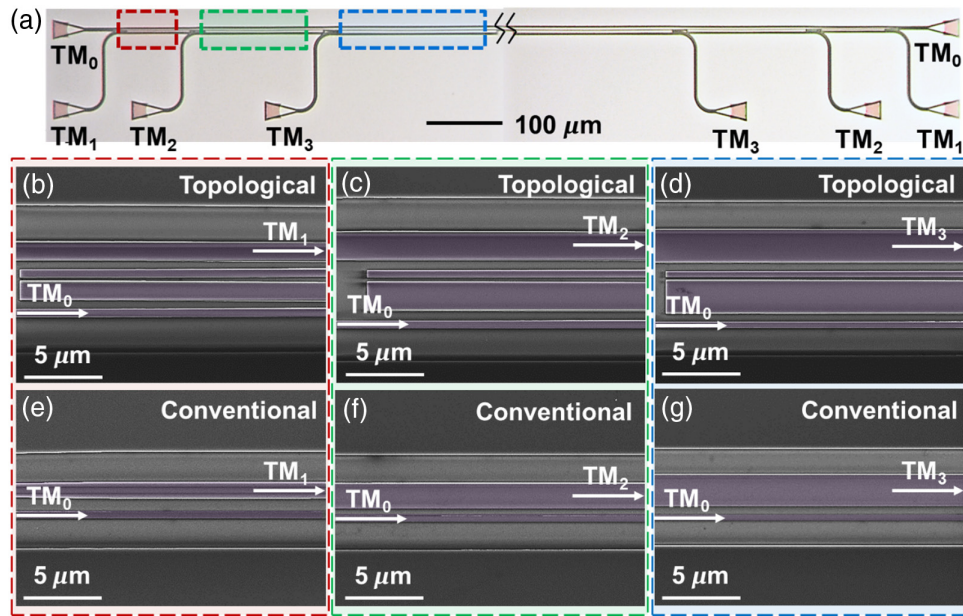


Fig. 4 Structures of the fabricated devices. (a) Optical microscope photo of the fabricated MDM device. The correspondence between the ports and the modes is indicated in the figure. The TM_0 -to- TM_1 , TM_0 -to- TM_2 , and TM_0 -to- TM_3 mode conversion regions are encircled by the red, green, and blue dashed boxes, respectively. (b)–(d) SEM images of the (b) TM_0 -to- TM_1 , (c) TM_0 -to- TM_2 , and (d) TM_0 -to- TM_3 mode-order converters based on the topological waveguide arrays. (e)–(g) SEM images of the (e) TM_0 -to- TM_1 , (f) TM_0 -to- TM_2 , and (g) TM_0 -to- TM_3 mode-order converters based on the conventional ADCs.

deposited over the devices by plasma-enhanced chemical vapor deposition. Figures 4(b)–4(d) display the scanning electron microscope (SEM) images of the waveguides in the TM_0 -to- TM_1 , TM_0 -to- TM_2 , and TM_0 -to- TM_3 mode conversion regions of the topological design, whereas Figs. 4(e)–4(g) present those of the conventional ADCs.

In the experiments, a tunable continuous wave laser and a photodetector were employed to measure the transmission spectra of the fabricated devices. The TM-polarized light was coupled into and out of the chip by grating couplers (GCs). The transmission spectra of the devices were normalized to that of the reference GCs fabricated on the same chip. More details about the experimental setup and the measurement methods can be found in Sec. S2 in the [Supplementary Material](#). Figure 5 shows the measured transmission spectra of the four-channel mode-division multiplexer employing the Thouless pumping mechanism with the light injected from the TM_0 to TM_3 ports on the left side of the device. Thanks to the broadband nature of the topological design, the measured ILs are lower than 0.4, 2.2, 2.4, and 2.6 dB over an 80-nm bandwidth (1500 to 1580 nm) for the TM_0 , TM_1 , TM_2 , and TM_3 mode channels, respectively. It means that the ILs of the TM_0 -to- $TM_{1,2,3}$ mode-order converters are less than 1.1, 1.2, and 1.3 dB, respectively. The measured CT values are below -23 , -23 , -20.5 , and -25 dB in the same wavelength range for the TM_0 - TM_3 mode inputs, respectively. As a comparison, the measured 3-dB bandwidth of the conventional mode-division multiplexer based on ADCs is only ~ 10 nm, and the CT value is less than -15 dB in the wavelength range of 1500 to 1580 nm (see Sec. S4 in the [Supplementary Material](#)). It confirms that the topological design is more robust

against wavelength variation compared with its conventional counterpart.

To evaluate the fabrication tolerance of the topological and conventional mode-division multiplexers, structural discrepancies were intentionally introduced to the waveguide width and the gap distance during the fabrication. Figure 6 shows

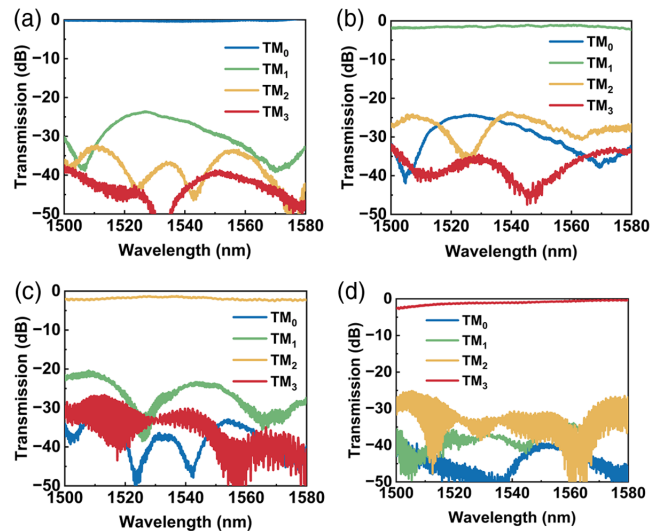


Fig. 5 Measured transmission spectra of the four modes when the light is injected from the (a) TM_0 , (b) TM_1 , (c) TM_2 , and (d) TM_3 input ports of the proposed topological MDM device.

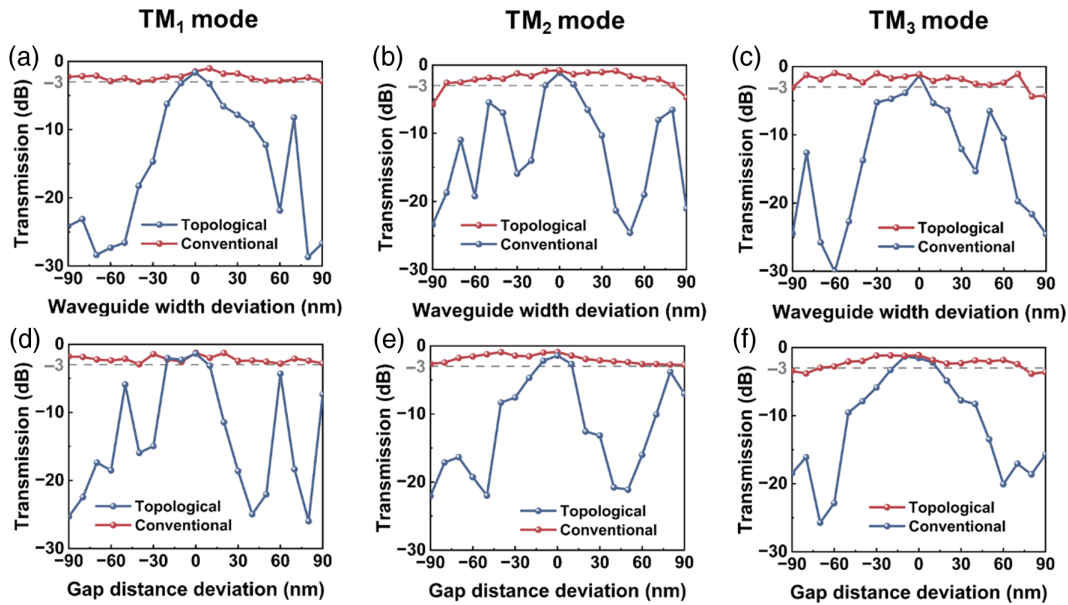


Fig. 6 Measured transmission of the target modes at 1550 nm of the fabricated topological and conventional mode-division multiplexers with various fabrication errors. (a)–(c) Measured transmission of the (a) TM_1 , (b) TM_2 , and (c) TM_3 modes when the waveguide width deviation δw varies from -90 to 90 nm. (d)–(f) Measured transmission of the (d) TM_1 , (e) TM_2 , and (f) TM_3 modes when the gap distance deviation δg varies from -90 to 90 nm.

the measured transmission of the target modes at 1550 nm when the waveguide width deviation δw or the gap distance deviation δg is varied in the range of -90 to 90 nm. The measured ILs of the topological device are kept below 3 dB even with large structural discrepancies (-90 to 90 nm for the TM_1 mode, -80 to 80 nm for the TM_2 mode, and -70 to 70 nm for the TM_3 mode), whereas the performance of the conventional device degrades significantly with the same fabrication errors. The larger ILs measured in the experiments compared with the values obtained in the simulations could be attributed to the fabrication imperfections such as waveguide sidewall roughness and partial filling of the gaps with the cladding material. The fabrication tolerance becomes worse with increasing mode order as the effective modal indices of high-order modes are close to each other and therefore more sensitive to the changes in structural parameters. Nevertheless, the experimental results clearly reveal that the topological design possesses great robustness against the structural deviations in waveguide width and gap distance, which has long been the pursuit of people working in this field. It is worth mentioning that the topological design method based on the Thouless pumping mechanism can also be applied to the on-chip mode manipulation for the transverse electric (TE) polarization (see Sec. S5 in the [Supplementary Material](#)). The topological devices working for TE modes have larger footprints and smaller feature sizes compared with their TM counterparts because the coupling strengths among TE modes are usually weaker than those among TM modes.

3.2 High-Speed Data Transmission Experiment

As proof of its possible application, we conducted a transmission experiment based on the four-channel topological MDM device by sending one high Baud rate signal to each channel at a time. Figures 7(a) and 7(b) illustrate the experimental setup

and transceiver digital signal processing (DSP) algorithms for high-speed transmission, respectively. A Nyquist-shaped 50-GBaud 16-QAM signal is transmitted through each channel of the MDM device. At the receiver, a real-valued multiple-input and multiple-output feedforward equalizer post filter, and maximum-likelihood sequence decision are employed to compensate for the transmission impairments. More detailed information for the experimental setup and DSP can be found in Sec. S2 in the [Supplementary Material](#). The measured optical spectra of 50-GBaud 16-QAM signals at different stages are shown in Fig. 7(c), with a resolution of 1.12 pm. Figure 7(d) plots the calculated BERs for the four mode channels, all below the 7% hard-decision forward error correction threshold of 3.8×10^{-3} . The recovered constellations of the 16-QAM signals for different modes are presented in Fig. 7(e), which indicates a good signal quality for all the channels. Note that the calculated BERs are well below the 7% FEC threshold, so the data rate can be further improved by increasing the data rate of the signal source and adding an optical bandpass filter after the second erbium-doped fiber amplifier (EDFA) to filter out the amplified spontaneous emission noises. Furthermore, the broadband and fabrication-tolerant properties of the topological mode manipulation can be exploited to build a larger-scale multiplexing system with more mode and wavelength channels, pushing the aggregate data rate of the system to a new level.

Table 2 compares the proposed device with several recently reported four-channel mode-division multiplexers.^{5,6,32–36} Our design achieves low ILs and CT values over a broad bandwidth, which shows great promise for applications in on-chip MDM datalinks. Benefitting from the topological nature of the Thouless pumping process, the mode conversion and multiplexing exhibit significant structural parameter insensitivity. To the best of our knowledge, our work has the highest fabrication tolerance among various types of silicon-based MDM devices,

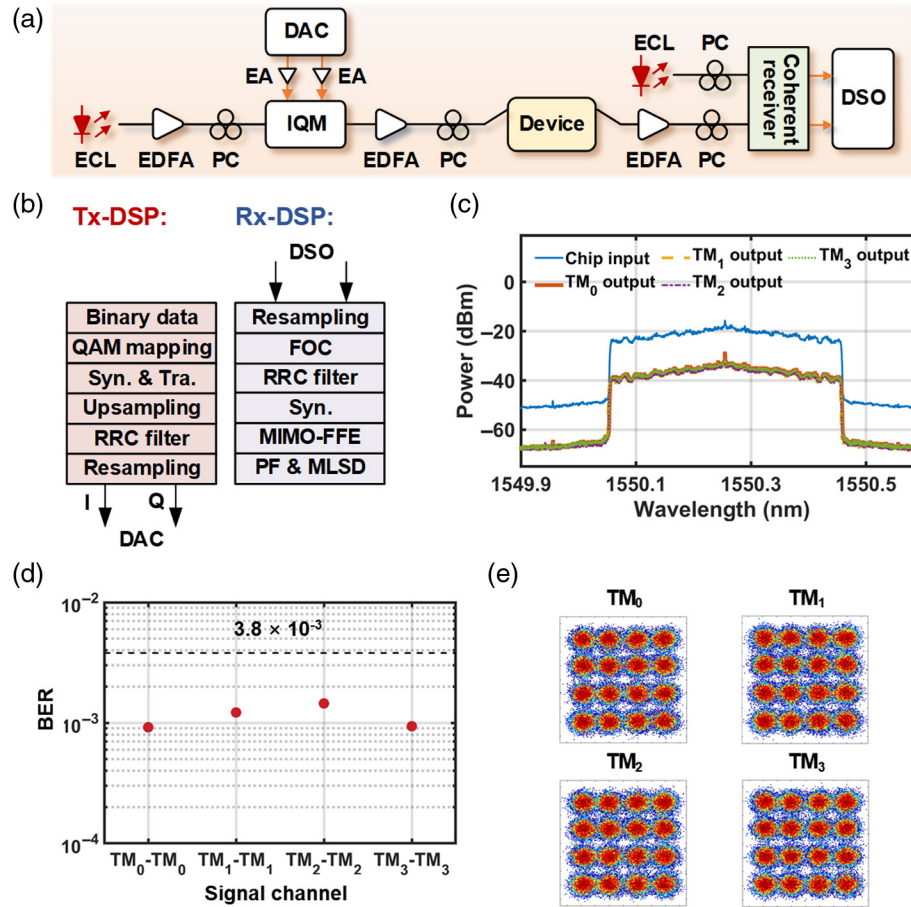


Fig. 7 High-speed data transmission experiment based on the four-channel topological MDM device. (a) Setup for the 200-Gb/s high data rate transmission experiment. The black and orange lines represent optical and electrical links, respectively. (b) DSP algorithms for the transceivers. (c) Measured optical spectra for the 16-QAM signals at different stages. (d) BERs for the four signal channels. (e) Recovered constellations for each mode.

Table 2 Comparison of various silicon-based four-channel MDM systems.

Ref.	Structure	Bandwidth (nm)	IL (dB)	CT (dB)	Fabrication tolerance
4	Shortcuts to adiabaticity	100	<1.3	<-23	±20 nm
5	ADCs	20	<4	<-23	—
32	Directional couplers with subwavelength sidewall corrugations	50	<4	<-16	±20 nm
33	Tilt waveguide junctions with shallow etched slots	60	<1.29	<-14.4	—
34	Pixelated waveguides	60	<3	<-14.6	±10 nm
35	Subwavelength grating-assisted triple-waveguide couplers	100	<5	<-10	±20 nm
36	Tapered ADCs	75	<6	<-16	±20 nm
This work	Topological waveguide arrays using the Thouless pumping mechanism	80	<2.6	<-20.5	±70 nm

which is very much desired in large-scale photonic integration and high-capacity optical communications.

4 Conclusion

To conclude, we have proposed and experimentally demonstrated a new method for wavelength- and structure-insensitive on-chip mode manipulation based on the RM-modeled silicon waveguide arrays. The Thouless pumping mechanism is exploited to realize robust mode couplings in the coupled-waveguide devices. Compared with other topological approaches, the Thouless pumping scheme employed in this work shows great robustness to the deviations not only in wavelength and gap distance but also in waveguide width, which contributes to the broadband and fabrication-tolerant properties of the topological devices. Using the proposed design method, we realize various high-efficiency mode-order conversions and construct a four-channel MDM system based on the topological waveguide arrays. The experimental results prove that the fabricated topological mode-division multiplexer has low ILs of < 2.6 dB and crosstalk of < -20.5 dB for the TM_0 to TM_3 MDM links over an 80-nm bandwidth (1500 to 1580 nm). Most importantly, the performance of the proposed device is topologically protected by the Thouless pumping mechanism, resulting in remarkable fabrication tolerance of ± 70 nm for the structural deviations in waveguide width and gap distance. To the best of our knowledge, this is the highest fabrication tolerance that has ever been reported in the coupled-waveguide mode-handling devices. All these merits are well confirmed in experiments by comparing the performance of the topological devices with that of the conventional ones based on ADCs. On the other hand, the adiabatic requirement of the Thouless pumps inevitably leads to larger device footprints compared with the conventional counterparts. It is really difficult to assess the compactness and the robustness at the same time because there is a trade-off between them. However, there are several new techniques emerging that could reduce the footprints of the topological devices based on the Thouless pumping mechanism. For example, the combination of a topological pump and coherent tunneling by adiabatic passage allows one to speed up the transfer process.³⁷ The adiabatic infimum of a topological pump can be approached by minimizing the effective Berry connection, leading to the Thouless pump with a rapid evolution speed.³⁸ Introducing next-nearest-neighbor coupling into the RM model is another method to engineer the quantum metric and lift the constraint of the slow evolution of the Thouless pumps, which gives rise to compact device footprints.³⁹ Moreover, the minimum feature size of the topological design is larger than 130 nm, indicating the possibility of its fabrication with foundry-compatible processes. A high-speed on-chip MDM data transmission experiment has also been successfully carried out with a data rate of 200 Gb/s per channel, which means the aggregate data rate would reach ~ 800 Gb/s. To the best of our knowledge, this is the first time robust transmission of data has been demonstrated using topological MDM devices. Further developments of this study could be envisaged, for example, the approach can also be applied to the mode manipulation for the TE polarization and perhaps more advanced mode- and polarization-division hybrid multiplexing devices. Our work provides an intriguing approach to relieving the wavelength sensitivity and improving the fabrication tolerance of coupled-waveguide devices, which would facilitate the development of diverse applications ranging from

optical communications^{23,24} and optical computing^{27,28} to nonlinear light generation⁴⁰ and quantum information processing.^{25,26,41}

Disclosures

The authors declare no conflicts of interest.

Code and Data Availability

Data underlying the results presented in this paper can be obtained from the authors upon reasonable request.

Acknowledgments

We would like to thank the Center for Advanced Electronic Materials and Devices of Shanghai Jiao Tong University for its support in device fabrication.

This work was supported by the National Key R&D Program of China (Grant No. 2023YFB2905503) and the National Natural Science Foundation of China (Grant Nos. 62035016, 62105200, 62475146, and 62341508).

References

1. H. Oukraou et al., "Broadband photonic transport between waveguides by adiabatic elimination," *Phys. Rev. A* **97**, 023811 (2018).
2. K. Chen et al., "Multimode 3 dB coupler based on symmetrically coupled waveguides for on-chip mode division multiplexing," *J. Lightwave Technol.* **35**, 4260–4267 (2017).
3. R. Alrifai et al., "Ultrabroadband beam splitting in a dissipative system of three waveguides," *Phys. Rev. A* **103**, 023527 (2021).
4. D. Guo and T. Chu, "Silicon mode (de)multiplexers with parameters optimized using shortcuts to adiabaticity," *Opt. Express* **25**, 9160–9170 (2017).
5. D. Dai, J. Wang, and Y. Shi, "Silicon mode (de)multiplexer enabling high capacity photonic networks-on-chip with a single-wavelength-carrier light," *Opt. Lett.* **38**, 1422–1424 (2013).
6. W. P. Su, J. R. Schrieffer, and A. J. Heeger, "Solitons in polyacetylene," *Phys. Rev. Lett.* **42**, 1698–1701 (1979).
7. Y. Guo, M. Xiao, and S. Fan, "Topologically protected complete polarization conversion," *Phys. Rev. Lett.* **119**, 167401 (2017).
8. S. Kruk et al., "Nonlinear light generation in topological nanostructures," *Nat. Nanotechnol.* **14**, 126–130 (2019).
9. M. A. Bandres et al., "Topological insulator laser: experiments," *Science* **359**, eaar4005 (2018).
10. W. Song et al., "Robust and broadband optical coupling by topological waveguide arrays," *Laser Photon. Rev.* **14**, 1900193 (2020).
11. W. Song et al., "Gauge-induced Floquet topological states in photonic waveguides," *Laser Photon. Rev.* **15**, 2000584 (2021).
12. J. Kang et al., "Topological photonic states in waveguide arrays," *Adv. Phys. Res.* **2**, 2200053 (2022).
13. D. J. Thouless, "Quantization of particle transport," *Phys. Rev. B* **27**, 6083–6087 (1983).
14. D. Xiao, M. C. Chang, and Q. Niu, "Berry phase effects on electronic properties," *Rev. Mod. Phys.* **82**, 1959–2007 (2010).
15. S. Nakajima et al., "Topological Thouless pumping of ultracold fermions," *Nat. Phys.* **12**, 296–300 (2016).
16. M. Lohse et al., "A Thouless quantum pump with ultracold bosonic atoms in an optical superlattice," *Nat. Phys.* **12**, 350–354 (2016).
17. Y. Ke et al., "Topological phase transitions and Thouless pumping of light in photonic waveguide arrays," *Laser Photon. Rev.* **15**, 2000584 (2021).
18. O. You et al., "Observation of non-Abelian Thouless pump," *Phys. Rev. Lett.* **128**, 244302 (2022).
19. M. Jürgensen et al., "Quantized fractional Thouless pumping of solitons," *Nat. Phys.* **19**, 420–426 (2023).

20. M. D. Schroer et al., “Measuring a topological transition in an artificial spin-1/2 system,” *Phys. Rev. Lett.* **113**, 050402 (2014).
21. W. Ma et al., “Experimental observation of a generalized Thouless pump with a single spin,” *Phys. Rev. Lett.* **120**, 120501 (2018).
22. L. Sun et al., “Broadband and fabrication-tolerant power coupling and mode-order conversion using Thouless pumping mechanism,” *Laser Photon. Rev.* **16**, 2200354 (2022).
23. Q. Xu et al., “Electrically tunable optical polarization rotation on a silicon chip using Berry’s phase,” *Nat. Commun.* **5**, 5337 (2014).
24. Z. Fan et al., “Mode-order conversion in a Mach–Zehnder interferometer based on Chern insulators,” *Opt. Lett.* **49**, 9–12 (2024).
25. L. Feng et al., “On-chip coherent conversion of photonic quantum entanglement between different degrees of freedom,” *Nat. Commun.* **7**, 11985 (2016).
26. L. Feng et al., “On-chip transverse-mode entangled photon pair source,” *npj Quantum Inf.* **5**, 2 (2019).
27. C. Wu et al., “Programmable phase-change metasurfaces on waveguides for multimode photonic convolutional neural network,” *Nat. Commun.* **12**, 96 (2021).
28. Z. Deng et al., “3-port beam splitter of arbitrary power ratio enabled by deep learning on a multimode waveguide,” *Opt. Laser Technol.* **169**, 109950 (2024).
29. M. J. Rice and E. J. Mele, “Elementary excitations of a linearly conjugated diatomic polymer,” *Phys. Rev. Lett.* **49**, 1455–1459 (1982).
30. A. Cerjan et al., “Thouless pumping in disordered photonic systems,” *Light Sci. Appl.* **9**, 178 (2020).
31. Y. E. Kraus et al., “Topological states and adiabatic pumping in quasicrystals,” *Phys. Rev. Lett.* **109**, 106402 (2022).
32. X. Wang et al., “Ultra-compact silicon mode (de)multiplexer based on directional couplers with subwavelength sidewall corrugations,” *Opt. Lett.* **47**, 2198–2201 (2022).
33. X. Guo et al., “Scalable and compact silicon mode multiplexer via tilt waveguide junctions with shallow etched slots,” *J. Lightwave Technol.* **40**, 4682–4688 (2022).
34. H. Xie et al., “Highly compact and efficient four-mode multiplexer based on pixelated waveguides,” *IEEE Photonics Technol. Lett.* **32**, 166–169 (2020).
35. W. Jiang et al., “Broadband silicon four-mode (de) multiplexer using subwavelength grating-assisted triple-waveguide couplers,” *J. Lightwave Technol.* **39**, 5042–5047 (2021).
36. H. Shu et al., “A design guideline for mode (de) multiplexer based on integrated tapered asymmetric directional coupler,” *IEEE Photonics J.* **11**, 6603112 (2019).
37. S. Longhi, “Topological pumping of edge states via adiabatic passage,” *Phys. Rev. B* **99**, 155150 (2019).
38. S. Wu et al., “Approaching the adiabatic infimum of topological pumps on thin-film lithium niobate waveguides,” *Nat. Commun.* **15**, 9805 (2024).
39. W. Song et al., “Fast topological pumps via quantum metric engineering on photonic chips,” *Sci. Adv.* **10**, eadn5028 (2024).
40. Y. Franz, J. Haines, and C. Lacava, “Strategies for wideband light generation in nonlinear multimode integrated waveguides,” *Phys. Rev. A* **103**, 013511 (2021).
41. L. Feng et al., “Transverse mode-encoded quantum gate on a silicon photonic chip,” *Phys. Rev. Lett.* **128**, 060501 (2022).
42. R. Citro and M. Aiderlsburger, “Thouless pumping and topology,” *Nat. Rev. Phys.* **5**, 87–101 (2023).
43. J. K. Asboth, L. Oroszlany, and A. Palyi, *A Short Course on Topological Insulators: Band-structure Topology and Edge States in One and Two Dimensions*, Springer Cham (2016).
44. C. Kittel and P. McEuen, *Introduction to Solid State Physics*, John Wiley & Sons (2005).
45. Y. Zhao et al., “Integrated broadband mode division demultiplexer in waveguide arrays,” *Phys. Rev. Appl.* **19**, 064014 (2023).
46. E. D. Palik, *Handbook of Optical Constants of Solids*, Academic Press (1998).

Lu Sun received his BS and doctor’s degrees from Shanghai Jiao Tong University, Shanghai, China, in 2011 and 2016, respectively. He was a postdoctoral fellow at the University of Toronto, Canada. He is now an associate professor at the Shanghai Jiao Tong University. His research interests include topological photonics, silicon photonics, and nanophotonics. He has published more than 50 journal and conference papers.

Biographies of the other authors are not available.